Design of a Wind Tunnel Balance using Topology Optimization Considering Multifunctional Stress Performance

Myung Kyun Sung[1] and Soobum Lee[2]
University of Maryland Baltimore County, Baltimore, MD, 21250, United States

Devin E. Burns[3]
NASA Langley Research Center, Hampton, VA, 23666, United States

This paper proposes a new topology optimization formulation for multifunctional performance of a compliant sensor structure – a wind tunnel balance. Compliant mechanism design is one of the main applications of topology optimization and plenty of successful design studies have been reported. However, design practicability is still questionable when stress concentration is critical due to complex/combined loads, especially at compliant hinge joints. In this paper, we formulate a new topology optimization formulation considering multiple loading scenarios in a compliant sensor structure design. Two separate constraints, one related to sensor performance and the other focused on structural safety in terms of maximum von Mises stress, are included in the design formulation. This formulation is to achieve excellent sensitivity of an applied axial load while maintaining structure safety with a combined general load applied which is one order higher than the axial load. This challenging problem is solved using a well-known SIMP approach with the relaxation and projection methods.

I. Introduction

Historically, topology optimization has been employed for designing lightweight and energy-efficient structure under specific density fraction [1–3]. It has been applied to design stiff structures under specific volume fraction constraints. One of the technical problems of topology optimization was manufacturability due to its complex design. As additive manufacturing (AM) technology has rapidly grown as one of the modern manufacturing solutions [4,5] and has overcome manufacturing issues, topology optimization has regained high attention as a structural design methodology. A few separate studies have been conducted to overcome realistic AM issues on overhang when topology optimization is applied – topology without supporting material by applying filtering method [6] and self-supporting structure [7].

Compliant mechanism design is another popular application of topology optimization. Compliant mechanism design is widely used for the precise force or displacement mechanisms [8] in microscale (MEMS: Micro Electro Mechanical System) and macroscale [9,10]. Sigmund [11] first introduced the topology optimization for compliant mechanism design to maximize a displacement, with plenty of follow up studies [12–14]. A strain gauge based load cell design has been proposed using compliant mechanism topology optimization [15]. One of the critical issues on using Solid Isotropic Microstructure with Penalization (SIMP) [16] – a well-known parameterization for topology optimization that obtains black and white design – is that it can produce one node connection designs. A one node connection is interpreted as a hinge joint that amplifies displacement, but this weak connection between elements in finite element analysis usually causes high-stress concentration and structural safety issues. A few remedies to avoid this weak connection and obtain a hinge free design are developed using a wavelet approach [17] or level set approach

[1] PhD student, Mechanical Engineering, msung1@umbc.edu
[2] Associate Professor, Mechanical Engineering, and AIAA Member Grade (if any), sblee@umbc.edu
[3] Force Measurement Engineer, Advanced Measurement and Data Systems Branch, Member AIAA.

[18]. More recently, stress-constrained topology optimization has been studied to remove one-node connection and highly stressed hinge in compliant mechanisms [19].

Development of topology optimization and additive manufacturing raises a fundamental design question if one can find a better structural design than the one believed to be the best design so far. A wind tunnel force balance, for example, is one of the important measurement devices that measure aerodynamic forces and moments experienced by wind tunnel models during wind tunnel testing. One of the well-accepted force balance designs is the internal type that is placed inside of the test model to predict the model's aerodynamic performance, and its design has seen limited updates in last century since first development [20,21]. A balance will simultaneously measure six force/moment components (F_x, F_y, F_z, M_x, M_y, M_z, axial force, normal force, side force, roll moment, yaw moment, pitch moment, respectively) while it provides the connection between the wind tunnel model and the sting that suspends the model in the tunnel flow. In this kind of force sensor, it is important to decouple multi-component forces for accurate measurement. To measure forces and moments accurately and simultaneously, researchers have tried to reduce the error using shape optimization [22,23], error reduction technique with signal processing [24], and machine learning [25].

Compared to a usual 6-axis force sensor, designing the force balance is challenging because of the axial force measurement section. Typically, an axial force is significantly smaller than other force components and hard to measure accurately. A traditional wind tunnel force balance measures the axial force from the deformation of vertical flexures [26–28]. On the axial section, strain gauges are attached to the vertical flexures and connected to a full Wheatstone bridge circuit to amplify the axial force signal and minimize the signal from other forces by mutual cancellation. Some researchers already made effort to measure the accurate axial force on the internal force balance using shape optimization for the vertical hinge [29], reduction of vertical flexure thicknesses [30], or modified Wheatstone bridge equation for interference error reduction [31]. However, previous studies are based on the traditional force balance shape and only minor shape design changes were considered. Also, they did not consider an extreme axial to normal force ratio – 1:6.25 [31], 1:4 [29,32] – unlike a high force ratio (1:10+) attempted in this study.

Stress analysis is essential part to evaluate the structural integrity of the balance. To solve the stress-based topology optimization effectively, some challenging problems need to be overcome [33]. First, singularity issue arises when elements are eliminated from the design domain due to zero density elements. Nonlinear optimization algorithms cannot generate subspaces that converge to local minima [34,35]. ε-relaxation [36] and q-p approach [37] have been introduced to overcome singularity issues and obtain smooth stress function in a design domain. The second problem is that stress values are fundamentally local properties. The adjoint method can be used for design sensitivity analysis to reduce computational time, but it is not suitable when one needs to handle element-wise stress measures as separated constraints due to its expensive computational time. To overcome local measurement issues, several methods to represent a local constraint as a global one have been introduced such as Kreisselmeier-Steinhauser function (KS Function) [38] and P-norm [39]. Both approaches, however, have convergence issues that are caused by infinite oscillation near convergence criteria [40]. Recently stability transformation method was presented to reduce the oscillation issue [41]. Normalization and interlacing methods were introduced to control maximum stress effectively [42]. Multi-P-norm formulation approach was proposed to remove a correction factor for P-norm [43]. Level set method has been reported to be able to control the maximum stress effectively, but requires more computational time [22,44].

This paper investigates the topology optimization of a force balance design that considers a high force ratio. In detail, we develop a new axial force measurement section for an internal wind tunnel balance using topology optimization that is possibly fabricated using additive manufacturing technology [45,46]. A new topology optimization formulation considers decoupling the balance responses from different forces and moment and maintaining structural safety. This design problem is challenging due to the extremely high force ratio (normal force is 13 times larger than axial force). Two separate design requirements are formulated as constraints: sensitivity to axial load and maximum von Mises stress under a threshold value. The axial load sensitivity is measured using local directional stress by the axial force at a sensor location (i.e. strain gauge), and the global maximum von Mises stress by the combined load (axial force + normal force + pitching moment) is used to evaluate structural safety. For global von Mises stress measurement, P-norm stress evaluation with relaxation method is used in this study. The rest of this paper is organized as follows: Section II introduces the topology optimization formulations for P-norm stress evaluation and directional stress. This section includes the design sensitivity analysis and filtering method. Section III presents a detailed discussion of the optimized designs. The final section concludes this study and presents future studies.

II. Optimization Problem

A. Problem Definition

This section defines the wind tunnel balance design problem. As explained in Introduction, the shape of a typical wind tunnel balance is a long solid rod mounted on a fixed base, and the other end is connected to the wind tunnel model. The design of the axial section is to be found in the middle of the rectangular domain as indicated in Figure 1. The design study handles a two-dimensional problem assuming the geometry and the loading is uniform through the thickness direction. Three loading conditions – axial force, normal force, and pitching moment – are applied to the center of the right edge, and Table 1 shows the magnitude of each component. The normal force is around 13 times larger than the axial force. To consider the problem in two dimensions, the forces and moment are normalized by thickness.

Table 1 Aerodynamic loads applied to the wind tunnel force balance

Load components	SI units*
Normal Force	116.8 N
Axial Force	8.9 N
Pitching Moment	7.43 Nm

* loads for unit thickness (mm)

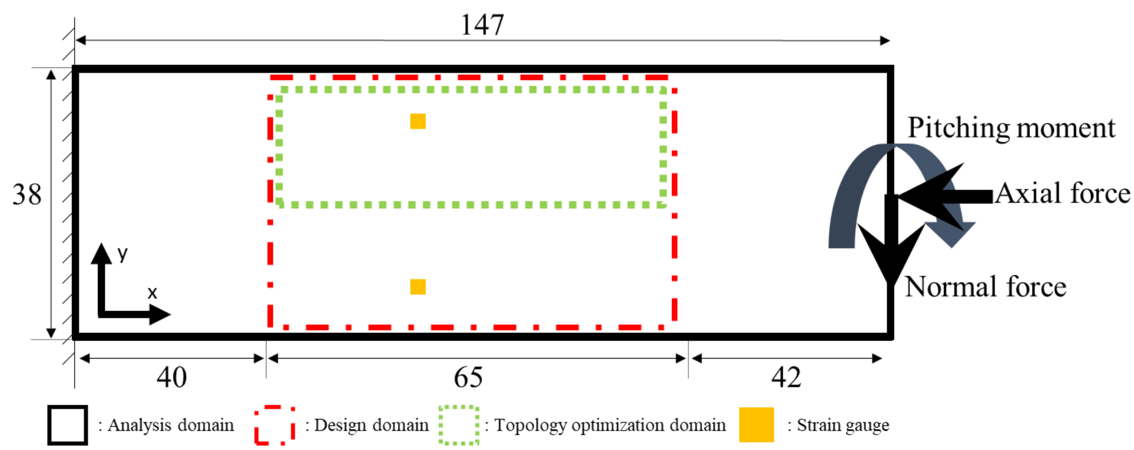

Fig.1 Boundary conditions for Problem – unit: mm

In this study, we define three different domains – analysis domain, design domain, and topology optimization domain. Figure 1 shows detail boundary conditions for this study. The analysis domain is an entire domain for the wind tunnel force balance analysis. The design domain is where we want to design for the axial force section. Bending stress cancellation between upper and lower half in a symmetric balance design is beneficial to minimize the bridge sensor output out of bending load. Therefore, we perform topology optimization for the upper part of the design domain only and mirror obtained topology to the lower part of the design domain. The detail design formulation will be explained in Section II.C. The rest of the analysis domain is assigned as passive elements (100% density throughout the optimization process).

Table 2 shows the maximum von Mises stress per wind tunnel safety allowable (for 300 maraging steel) and the minimum stress (directional) that should be detected by the axial force sensor when axial force is applied. The maximum von Mises stress is measured when the combined force (axial + normal + pitching moment) are applied to the balance, to consider required structural safety.

Table 2 Stress conditions for the force balance

Stress Condition	SI units
Maximum von Mises stress	0.896 GPa
Minimum Sensor Performance (σ_0)	75 MPa

B. Stress measures

In this paper, we used two different stress measures – P-norm stress with relaxation method for structural safety allowance which is maximum of global stress evaluation, and the directional stress for the sensor performance. The P-norm stress is evaluated using the following equation:

$$\sigma_{pnorm} = \left[\sum_{i=1}^{n} v_i \tilde{\sigma}_i^{Pn} \right]^{1/Pn} \tag{1}$$

where i is element index, n is the number of elements, v_i is elemental volume, Pn is norm parameter, and the tilde indicates a relaxed stress. The P-norm stress controls the level of the overall structural stress by taking the tendency of the stress. That is, the P-norm stress with the infinity norm parameter ($Pn = \infty$) represents the maximum von Mises stress of the structure. However, a larger norm parameter causes a higher degree of non-linearity and discontinuity of the optimization process that finds local minima. The norm parameter requires adjustment to obtain a feasible solution close to the global minimum. In this study, the norm parameter is adjusted by trial and error as 2.5 ($Pn = 2.5$) that works effectively for stable optimization convergence. Relaxation method is applied to design variables to generate a smooth feasible design domain and to overcome the singularity issue. The relaxed von Mises stress at element i is formulated as:

$$\tilde{\sigma}_i = x_i^{r-P} \sigma_{VM,i} \tag{2}$$

where x_i is the element-wise density variable, r is relaxation power, P is penalization power for SIMP approach, and $\sigma_{VM,i}$ is elemental von Mises stress. The study on the effect of these parameters is not a focus of this paper, but one can find an in-depth study by Le et al. [42]. P=3 and r=0.5 are used for this study. For more information, a sensitivity analysis is included in Appendix.

C. Optimization Formulation

The topology optimization problem for the axial section of a wind tunnel balance design is formulated as:

$$\min \; : \sigma_{pnorm} = \left[\sum_{i=1}^{n} v_i \tilde{\sigma}_i^{Pn} \right]^{1/Pn} \tag{3}$$

$$s.t. \quad : \mathbf{Ku} = \mathbf{f} \tag{4}$$

$$: \left| \frac{\sigma_{su}(\mathbf{x}) + \sigma_{sl}(\mathbf{x})}{2} \right| \geq \sigma_0 \qquad by\, \mathbf{F}_a \tag{5}$$

$$: \left[\sum_{i=1}^{n} v_i \tilde{\sigma}_i^{Pn} \right]^{1/Pn} \leq \sigma_{safe} \qquad by \sum \mathbf{F} \tag{6}$$

where **K** is a global stiffness matrix, **u** is a global displacement vector and **f** is a global force vector. **f** is either the axial force ($\mathbf{F}_a$) for evaluation of sensing performance, or the combined force ($\Sigma\mathbf{F} = \mathbf{F}_a + \mathbf{F}_n$ (normal force) + $\mathbf{M}_p$ (pitching moment)) for evaluation of maximum von Mises stress. σ_{su} and σ_{sl} are local directional stress on the sensor location, upper and lower location, respectively. σ_0 is the minimum sensor performance requirement under the axial force. This formulation includes two inequality constraints that consider two functional requirements of the wind tunnel balance in Table 2 (minimum sensor performance and maximum von Mises stress). To obtain the sensor performance, we apply the Wheatstone bridge circuit on the force balance that averages two axial stresses. The symmetric domain setup in Figure 1 ensures stress value cancellation when the structure experiences bending deformation. Therefore, the sensor performance by the combined force is not considered in the formulation. To consider the maximum von Mises stress, we formulated the constraint of the P-norm to be smaller than the threshold σ_{safe} = 2 that corresponds to the maximum von Mises stress 0.896 GPa (found by trial and error). In addition, the objective function is chosen to minimize stress P-norm function. This formulation is to achieve a feasible balance design as defined in Table 2 regarding stress performances, and to obtain a durable structural design represented by minimum P-norm stress. Method of Moving Asymptotes (MMA) is used for the optimization algorithm.

D. Projection Method

For the formulation, we employ a projection method to obtain clear black and white topological design results. A filtering method is introduced to avoid checkerboard pattern that is caused by numerical instabilities and non-convergence of finite element solution [47,48]. Density filtering [49] and sensitivity filtering [11] are popular among others, but they may cause intermediate density or artificial material (grey area) that makes it difficult to discern a clear structural boundary for easy manufacture. If grey elements are involved in stress-based topology optimization, it can amplify a displacement and overestimate the stress value compared to black and white solutions. The projection method is one such filtering method. It was used to achieve minimum length that is applied on nodal design variables [50], and modified to consider elemental design variables [51].

In this study, a smoothed Heaviside function for elemental design variable is applied for projection method as:

$$\bar{x}_i = \frac{\tanh(\beta\eta) + \tanh(\beta(\tilde{x}_i - \eta))}{\tanh(\beta\eta) + \tanh(\beta(1-\eta))} \tag{7}$$

where $\bar{x}_i$ is the physical variable of element i, $\tilde{x}_i$ is intermediate filtered density corresponding to x_i which is the design variable. β determines the slope of the Heaviside curve, and η is the threshold point. If the intermediate density is less than η, it is projected into 0. Otherwise, it is projected into 1. Generally, topology optimization is initiated with a small valued β (e.g. 1) and updated every specific iteration (e.g. every 50 iterations) or when an iterative design variable change is less than 1%. Starting with a large β is proposed for the MMA algorithm by tightening two initial asymptotes of the MMA [52]. This method is effective to prevent perturbation of design variables and slow convergence. We start with a small β (=1) for a moderate tightening of the asymptotes that brings better topology design. β is updated every 150 iterations or when the density-changing ratio is less than 0.1%. β is increased up to 64 and η is fixed as 0.5.

The intermediate density is obtained using the density filter as below:

$$\tilde{x}_i = \frac{1}{\sum_{e \in N_i} H_{ie}} \sum_{e \in N_i} H_{ie} x_e \tag{8}$$

where e is the element index located within the filter radius r_{min} from element i, and H_{ie} is a weight factor as below:

$$H_{ie} = \max(0, r_{\min} - \Delta(i,e)) \tag{9}$$

where $\Delta(i,e)$ is the center to center distance between element i and element e.

The sensitivity with respect to a design variable is determined using the chain rule [51]:

$$\frac{\partial f}{\partial x_i} = \frac{\partial f}{\partial \bar{x}_i} \frac{\partial \bar{x}_i}{\partial \tilde{x}_i} \frac{\partial \tilde{x}_i}{\partial x_i} \tag{10}$$

As mentioned in Section II.A,topology optimization is performed considering geometric symmetry between the upper and lower domains. That is, the density design variables are updated for the upper and the lower domain at the same time. Therefore, the sensitivity should consider the design change in both the upper and lower domains. At element i, the final sensitivity considering design symmetry can be formulated as:

$$\frac{\partial f}{\partial x_{i,final}} = \frac{\partial f}{\partial x_i} + \frac{\partial f}{\partial x_{i,l}} \tag{11}$$

where f is a general function, $x_{i,l}$ represents the elements symmetrically located to x_i. x_i and $x_{i,l}$ are at the same horizontal location, but symmetrically located along the vertical direction – if element x_i is located on the top surface, element $x_{i,l}$ is located on the bottom surface of the design domain.

III. Design study results and analysis

This section explains the results of a design study that focuses on finding the optimal balance topology considering variable sensor locations. Again, this study considers two major concerns: the sensor performance under the axial force and the structural safety under the combined force. Due to high computational cost, we perform the topology optimization for ten (10) different sensor locations (A to J in Figure 4) rather than scanning all possible locations. We use a 4-noded rectangular element with 0.333mm^2 element size for the finite element method. Total number of elements is 50274 in the analysis domain, and 22230 elements are used design domain. The force values in Table 1 are used for this design study. Vertical (y) directional stress is used for evaluating the sensor performance. Table 3 summarizes the optimization parameters used in this Section.

Table 3 Parameters used in topology optimization

Description	Parameter	Value
Filter radius	r_{min}	1.332 mm
Young's modulus	E_0	189 GPa
Poisson's ratio	γ	0.3
Norm parameter for P-norm	Pn	2.5
relaxation power	r	0.5
Penalization power	P	3.0
Threshold for maximum P-norm	σ_{safe}	2.0
Minimum directional stress for sensor performance	σ_0	75 MPa
Slope for Heaviside function	β	Initially 1; increased up to 64
Threshold point for the Heaviside function slope	η	0.5

The locations in Figure 4 present one sensor located in the upper topology optimization design domain. The second sensor is located symmetrically in the lower design domain.

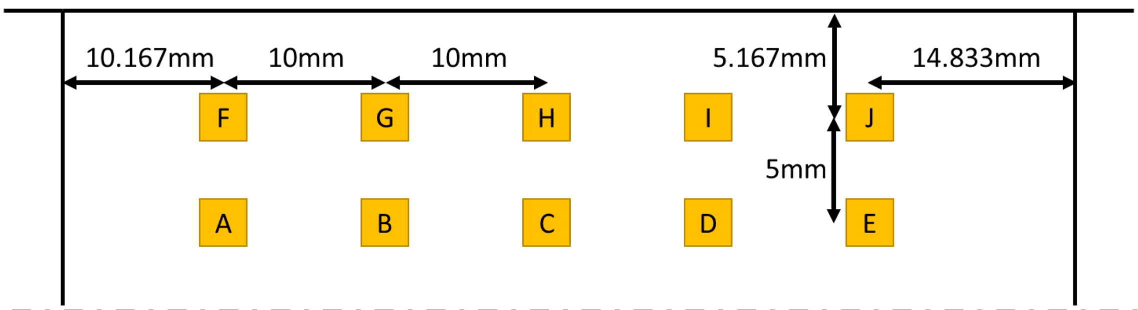

Fig. 4 Different sensor locations in the topology domain

Out of ten separate topology optimization runs, two feasible solutions are obtained for sensor locations C and G as shown in Figure 5 after 2500 iterations where a user-defined convergence criterion is met (maximum x_i change less than 0.1%). In these cases, there is no grey area found and all the performance requirements are satisfied as shown in Table 4. In each subfigure, the green (on the top) and blue (on the bottom) circles indicate the sensor locations and the red circle (on the right) indicates maximum von Mises stress location. Their exact locations are provided in Table 4.

(a) Design C

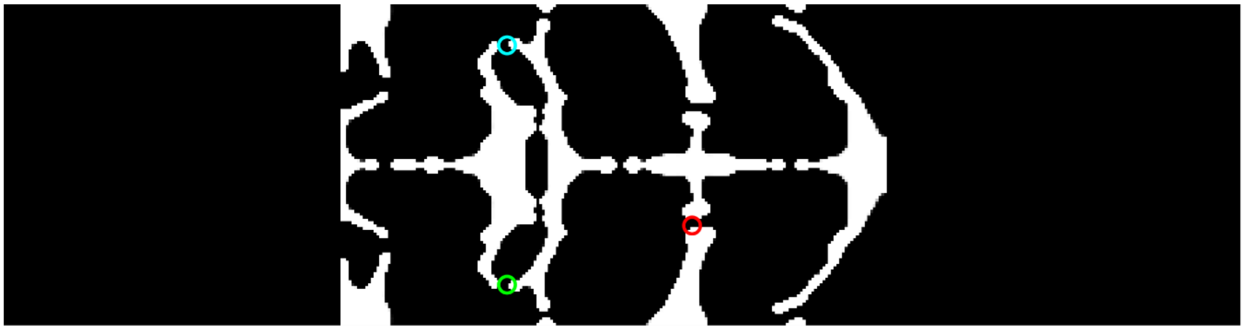

(b) Design G

Fig. 5 Design examples using topology optimization

Table 4 Stress measures for Design C and G

Stress (MPa)	Sensor performance (blue circle)		Max von Mises stress (red circle)	
	Top sensor location*	**value**	**Location***	**value**
Design C	(30.167, 10.167)	75.0	(44.167, 19.500)	856
Design G	(20.167, 5.167)	77.9	(42.167, 26.500)	813
Requirement	≥ 75.0		≤ 896	

* measure from top/left corner of design domain to the center of the sensor element (mm)

A detailed analysis is performed for these two designs in this section. Figure 6 shows the histories of the maximum von Mises stress (solid line) and the sensor performance (dash-dotted line) of Design C. The circles on the graph indicate β updating point (=every 150 iterations) for projection method. The graphical topology change is illustrated in Figure 7(a). In Figure 6, sudden changes of both the maximum von Mises stress and the sensor performance are observed when β is updated. As mentioned in Section 2.5, β update makes the physical variables mapped closer to its extremes (zero or one). The updated β causes sudden changes of the density variable close to the threshold (η = 0.5) that result in the jumps of stress measures. As iterations continue, however, the number of density variables close to the threshold decreases and the overall design process becomes stable. Another reason for sudden change for the maximum von Mises stress is due to its location change. For example, a sharp drop of the von Mises stress around iteration 600 is because of the location change as shown in Figure 7 (a). Several sharp peaks are due to design perturbation by the MMA.

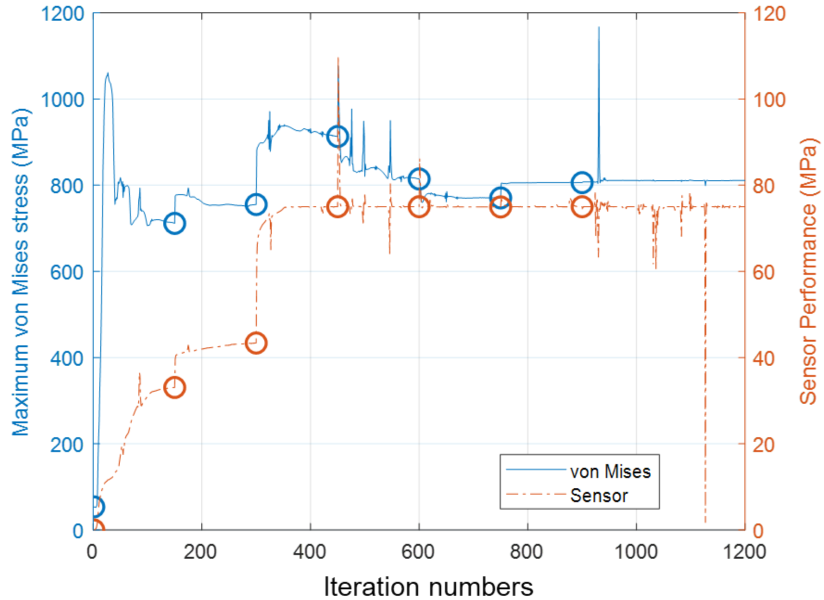

Fig. 6 Maximum von Mises stress and sensor performance histories of Design C

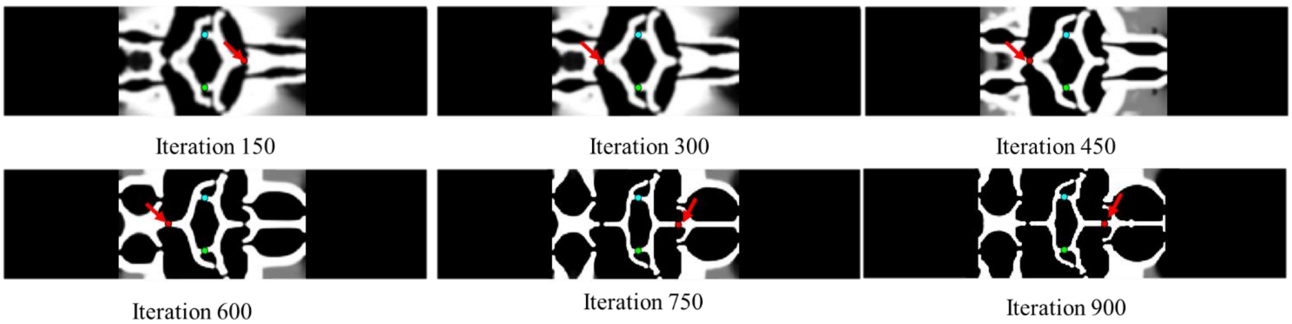

(a) Design C

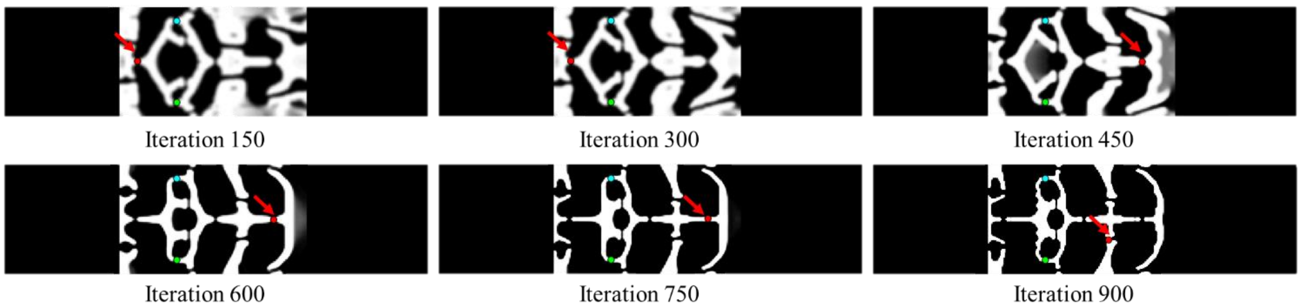

(b) Design G

Fig. 7 History of maximum von Mises stress location (indicated by arrow)

A. Mechanism analysis and verification study

This section analyzes the balance design mechanisms and conducts a verification study for Design C. Figure 8 is the deformed shape and the directional stress (vertical direction) contour for Design C subject to axial force. The arrows in Figure 8 (a) indicate deformation directions. A close observation reveals that the mechanism layout is symmetric horizontally – Bodies 1 and 6 convey compressional force to Bodies 2 and 5 that are supported by hinged joints a and b. The rotational motion of bodies 2 and 5 vertically extends the internal links composed of Bodies 3 and 4. The angled configuration between bodies 3 and 4 enables the extending deformation after the force is applied, and the sensor located between bodies 3 and 4 experiences bending (tensional) stress. In general, stress and deformation are concentrated at the hinged joints.

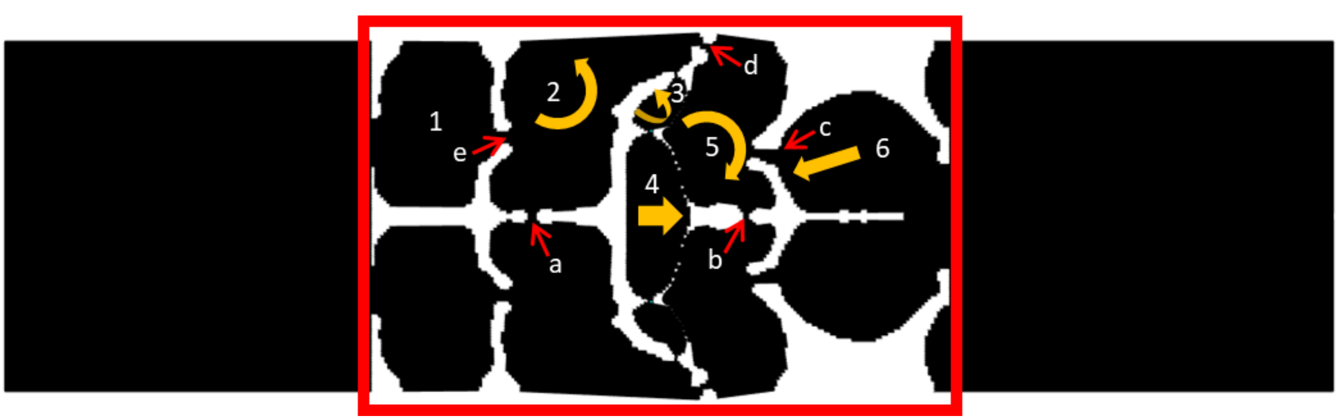

(a) Deformed shape with movement direction

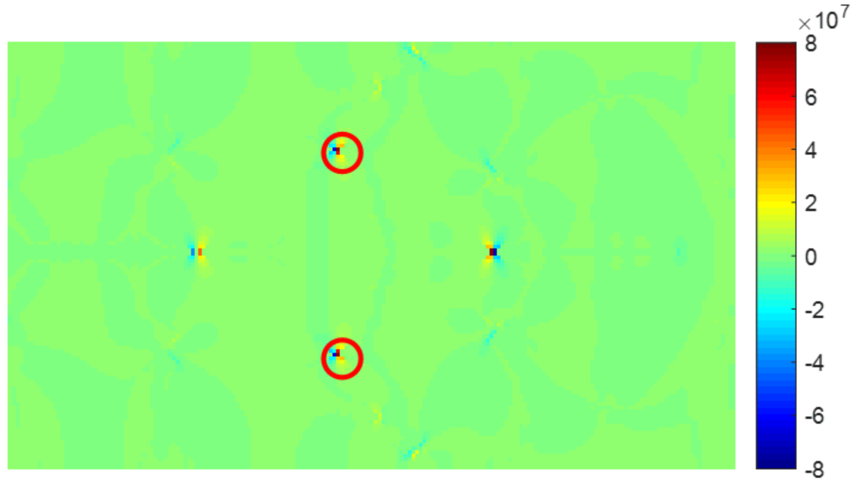

(b) Vertical directional stress contour for the design domain (circle: sensor locations)

Fig. 8 Sensor performance analysis for Design C under the axial force

The von Mises stress distribution for Design C subject to combined load is presented in Figure 9 where the largest stress values are found close to the hinged joints. The maximum von Mises stress is found at Joint b (856 MPa). However, one can observe that the stress at the sensor locations is well suppressed.

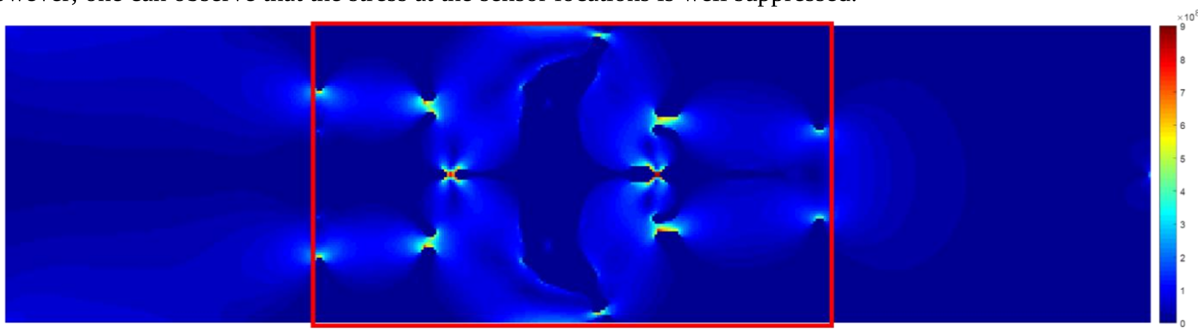

Fig. 9 von Mises stress contour under the combined load for Design C

Analysis study has been performed to justify this unique geometry. First, to understand the need for a slot under body 6, we modified the topology optimization result on Design C by filling the slot as shown in Figure 10 (highlighted area). In the optimized design (Figure 8), body 5 needs to rotate centered at Joint b and have a vertical deformation on Joint d that is enabled by moving down Joint c. A modified design (Figure 10) was explored that constrains the vertical deformation of Joint c that hinders the rotational movement of body 5. As a result, the directional stress is decreased on the sensor location from 75 MPa for the optimal results to 73 MPa.

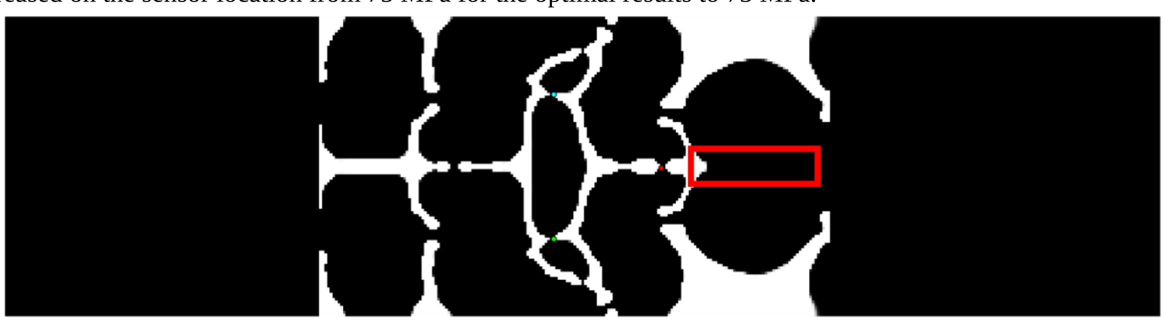

Fig. 10 Modified design (filled slot) for Design C

The design with the slot is also justified for the von Mises stress design criterion when the combined load is applied. The changed design in Figure 10 has the maximum von Mises stress slightly increased (858MPa) on the same location

(Joint b). The horizontal displacement at Joint d is decreased (252.7 → 252.4 mm), but the vertical displacement is increased (-587.7 → -588.4 mm). This larger rotational motion by body 5 makes higher von Mises stress on Joint b.

An additional verification study was conducted to understand the effect of the stiffness on Joint e between body 1 and body 2 on Design C. Table 5 shows the location of the maximum von Mises stress (arrow) by different thicknesses of joint e, and Table 6 shows the effect of the hinge thickness on the stress value changes.

Table 5 Maximum von Mises stress location under different hinge thickness

	Original	Thicker	Thinner
Design C			

Table 6 Effect of the thickness of a hinge between Body 1 and 2

Units (MPa)	Original design	Thicker hinge (200%)	Thinner hinge (50%)
Max von Mises stress	856	853	1208
Sensor performance	75	62.7	80.6

As analyzed previously, a thicker joint limits flexibility to improve the maximum von Mises stress performance, but makes the sensor performance unsatisfied. In addition, the thickness change causes the change of the location for maximum von Mises stress. To summarize, the design found in this study have the optimal joint thicknesses and locations to satisfy both sensor performance and structural safety.

IV. Conclusion

In this study, we performed stress-based topology optimization to satisfy design requirements for an internal wind tunnel balance. P-norm stress evaluation is introduced to consider the location-varying maximum von Mises stresses. Directional stress evaluation is used to obtain the sensor performance. To eliminate grey area, the projection method is implemented for the topology optimization. Compliant mechanism designs are obtained to satisfy requirements of the internal wind tunnel balance that considers two different loading conditions: axial and combined load. This balance design is challenging because it is required to have (1) substantial stress reading by the axial force that is more than one order smaller than the combined load and (2) the maximum stress by the combined load has to be less than the safety target. The optimization problem is formulated to consider both stress requirements. As a result, all hinges in the compliant balance mechanisms are found to have appropriate thickness and lengths to assure both the sensor performance and structural safety.

For more practical balance design, it is required to consider the dimension of the actual strain gauge sensor in the design process. Future works include extending the methodology to the 3D topology optimization with more focus on manufacturability (e.g., minimum feature length).

Appendix

A. Sensitivity Analysis

The sensitivity formulation of the elemental stress component as well as von Mises stress is derived using the SIMP approach in this section. First, an unrelaxed elemental von Mises stress is evaluated as:

$$\sigma_{VM,i}^2 = \sigma_i{}^T \mathbf{V} \sigma_i = \mathbf{q}_i{}^T \mathbf{M} \mathbf{q}_i \tag{1}$$

$$\sigma_i = x_i^P \mathbf{C_0} \mathbf{B} \mathbf{q}_i \tag{2}$$

$$\mathbf{V}=\begin{bmatrix} 1 & -1/2 & 0 \\ -1/2 & 1 & 0 \\ 0 & 0 & 3 \end{bmatrix} \tag{3}$$

where $\mathbf{V}$ is the Voigt matrix, $\sigma_i = \{\sigma_{11}, \sigma_{22}, \sigma_{12}\}^{\mathrm{T}}$ is the two dimensional stress vector component, $\mathbf{q}_i$ is nodal displacement vector for element i, $\mathbf{C_0}$ is elasticity tensor, $\mathbf{B}$ is strain displacement matrix ($\boldsymbol{\varepsilon}_i=\mathbf{B}\mathbf{q}_i$), and $\mathbf{M} = \mathbf{T}^T\mathbf{V}\mathbf{T}$ with $\mathbf{T} = x_i^P\mathbf{C_0}\mathbf{B}$.

The sensitivity for the von Mises stress can be derived using its squared expression as follows:

$$\begin{aligned}
\frac{\partial}{\partial x_i}\left(\sigma_{VM,i}^2\right) &= \frac{\partial}{\partial x_i}\left(\mathbf{q}_i^T\mathbf{M}\mathbf{q}_i\right) = \mathbf{q}_i^T\,\frac{\partial \mathbf{M}}{\partial x_i}\mathbf{q}_i + 2\mathbf{q}^T\mathbf{M}\frac{\partial \mathbf{q}_i}{\partial x_i} \\
&= \mathbf{q}_i^T\,\frac{\left(2P\,\mathbf{T}^{\mathbf{t}}\mathbf{V}\mathbf{T}\right)}{x_i}\mathbf{q}_i + 2\mathbf{q}^T\mathbf{M}\frac{\partial \mathbf{q}_i}{\partial x_i} \\
&= \frac{2P\left(\sigma_{VM,i}^2\right)}{x_i} + 2\mathbf{q}^T\mathbf{M}\frac{\partial \mathbf{q}_i}{\partial x_i}
\end{aligned} \tag{4}$$

The relationship of two sensitivities for the von Mises stress and its square is rewritten as

$$\frac{\partial}{\partial x_i}\left(\sigma_{VM,i}^2\right) = 2\sigma_{VM}\,\frac{\partial \sigma_{VM,i}}{\partial x_i} \tag{5}$$

$$\frac{\partial \sigma_{VM,i}}{\partial x_i} = \frac{1}{2\sigma_{VM,i}}\frac{\partial}{\partial x_i}\left(\sigma_{VM,i}^2\right) \tag{6}$$

Combining Eqs. (4) and (6), the sensitivity for elemental von Mises stress is written as

$$\begin{aligned}
\frac{\partial \sigma_{VM,i}}{\partial x_i} &= \frac{1}{2\sigma_{VM,i}}\left[\frac{2P}{x_i}\sigma_{VM,i}^2 + 2\mathbf{q}^T\mathbf{M}\frac{\partial \mathbf{q}_i}{\partial x_i}\right] \\
&= \frac{P}{x_i}\sigma_{VM,i} + \frac{1}{\sigma_{VM,i}}\mathbf{q}^T\mathbf{M}\frac{\partial \mathbf{q}_i}{\partial x_i}
\end{aligned} \tag{7}$$

Then, the sensitivity for the P-norm stress is evaluated as follows:

$$\sigma_{pnorm} = \left[\sum_{i=1}^{n} v_i\tilde{\sigma}_i^{Pn}\right]^{1/Pn} \tag{8}$$

$$\frac{\partial \sigma_{pnorm}}{\partial x_i} = \sigma_{pnorm}{}^{1-Pn}\left[r\frac{v_i\tilde{\sigma}_i^{Pn}}{x_i} + \sum_{i=1}^{n}\left(\frac{v_i\tilde{\sigma}_i^{Pn}}{\sigma_{VM}^2}\mathbf{q}_i^T\mathbf{M}\frac{\partial \mathbf{q}_i}{\partial x_i}\right)\right] \tag{9}$$

where r is relaxation power. To calculate displacement with respect to design variable ($\partial\mathbf{q}_i/\partial x_i$), the adjoint method is used. Assuming loads are design independent, or $\partial\mathbf{f}/\partial x_i = 0$. For convenience, $\sigma_{pnorm}{}^{1-Pn}$ is multiplied on the adjoint term as:

$$\mathrm{L} = \sigma_{pnorm} + \boldsymbol{\lambda}^T(\mathbf{Ku}-\mathbf{f})\sigma_{pnorm}{}^{1-Pn} \tag{10}$$

Its partial derivative with respect to the design variable leads to:

$$\frac{\partial \mathrm{L}}{\partial x_i} = \sigma_{pnorm}{}^{1-Pn}\left[r\frac{v_i\tilde{\sigma}_i^{Pn}}{x_i} + \sum_{i=1}^{n}\frac{v_i\tilde{\sigma}_i^{Pn}}{\sigma_{VM}^2}\mathbf{q}^T{}_i\mathbf{M}\frac{\partial \mathbf{q}_i}{\partial x_i} + \boldsymbol{\lambda}^T\left(\frac{\partial \mathbf{K}}{\partial x_i}\mathbf{u} + \mathbf{K}\frac{\partial \mathbf{u}}{\partial x_i} - \cancel{\frac{\partial \mathbf{f}}{\partial x_i}}\right)\right]$$
$$= \sigma_{pnorm}{}^{1-Pn}\left[r\frac{v_i\tilde{\sigma}_i^{Pn}}{x_i} + \boldsymbol{\lambda}^T\frac{\partial \mathbf{K}}{\partial x_i}\mathbf{u} + \left(\sum_{i=1}^{n}\frac{v_i\tilde{\sigma}_i^{Pn}}{\sigma_{VM}^2}\mathbf{q}^T{}_i\mathbf{M}\mathbf{R}_i + \boldsymbol{\lambda}^T\mathbf{K}\right)\frac{\partial \mathbf{u}}{\partial x_i}\right] \tag{11}$$

where $\mathbf{R}_i$ is a restriction matrix that satisfied $\mathbf{q}_i = \mathbf{R}_i\,\mathbf{u}$.
Finally, the sensitivity for the P-norm stress with respect to the design variable x_i is expressed as:

$$\frac{\partial \sigma_{pnorm}}{\partial x_i} = \frac{\sigma_{pnorm}{}^{1-Pn}}{x_i}\left[r v_i\tilde{\sigma}_i^{Pn} + P\boldsymbol{\lambda}^T x_i^P\mathbf{K}_{e,i}\mathbf{q}_i\right] \tag{12}$$

where $\mathbf{K}_{e,i}$ is elemental stiffness that satisfies $\mathbf{K}_{e,i} = \int_{v_i}\mathbf{B}^T\mathbf{C}_0\mathbf{B}\,dv_i$ where v_i is elemental volume, and the adjoint equation is defined as:

$$\mathbf{K}\boldsymbol{\lambda} = -\sum_{i=1}^{n}\frac{v_i\tilde{\sigma}_i^{Pn}}{\sigma_{VM}^2}\mathbf{q}^T{}_i\mathbf{M}\mathbf{R} \tag{13}$$

The sensitivity for the directional stress is derived similarly using the adjoint method [53]. First, a directional stress component in element j (σ_j) is written as:

$$\sigma_j = x_j^P\mathbf{C_0}\mathbf{B}\mathbf{R}_j\mathbf{u} \tag{14}$$

Same as the P-norm stress evaluation, the loads are design independent ($\partial\mathbf{f}/\partial x_i = 0$). The adjoint method for directional stress is as below:

$$\mathrm{L} = \sigma_j + \boldsymbol{\lambda}^T(\mathbf{K}\mathbf{u} - \mathbf{f}) \tag{15}$$

$$\frac{\partial \mathrm{L}}{\partial x_i} = \frac{\partial \sigma_j}{\partial x_i} + \boldsymbol{\lambda}^T\mathbf{K}\frac{\partial \mathbf{u}}{\partial x_i} + \boldsymbol{\lambda}^T\frac{\partial \mathbf{K}}{\partial x_i}\mathbf{u} - \cancel{\boldsymbol{\lambda}^T\frac{\partial \mathbf{f}}{\partial x_i}}$$
$$= \delta_{ij}P x_i{}^{P-1}\mathbf{C_0}\mathbf{B}\mathbf{R}_j\mathbf{u} + \left(x_j^P\mathbf{C_0}\mathbf{B}\mathbf{R}_j + \boldsymbol{\lambda}^T\mathbf{K}\right)\frac{\partial \mathbf{u}}{\partial x_i} + \boldsymbol{\lambda}^T\frac{\partial \mathbf{K}}{\partial x_i}\mathbf{u} \tag{16}$$

Therefore, the sensitivity for the directional stress component is written as:

$$\frac{\partial \sigma_j}{\partial x_i} = \delta_{ij}P x_i{}^{P-1}\mathbf{C_0}\mathbf{B}\mathbf{R}_j\mathbf{u} + P\boldsymbol{\lambda}^T x_i^{P-1}\mathbf{K}_e\mathbf{q}_i \tag{17}$$

where the adjoint load $\boldsymbol{\lambda}$ is defined as:

$$\mathbf{K}\boldsymbol{\lambda} = -x_j^P\mathbf{C_0}\mathbf{B}\mathbf{R} \tag{18}$$

Acknowledgments

The authors gratefully acknowledge NASA Langley Research Center and the National Institute of Aerospace for their support from Prime Contract No. NNL13AA08B, Subcontract No. T19-601049-UMBC.

References

[1] Bendsøe, M. P., and Kikuchi, N. “Generating Optimal Topologies in Structural Design Using a Homogenization Method.” *Computer Methods in Applied Mechanics and Engineering*, Vol. 71, No. 2, 1988, pp. 197–224. https://doi.org/http://dx.doi.org/10.1016/0045-7825(88)90086-2.

[2] Andreassen, E., Clausen, A., Schevenels, M., Lazarov, B. S., and Sigmund, O. “Efficient Topology Optimization in MATLAB Using 88 Lines of Code.” *Structural and Multidisciplinary Optimization*, Vol. 43, No. 1, 2011, pp. 1–16. https://doi.org/10.1007/s00158-010-0594-7.

[3] Sigmund, O. “A 99 Line Topology Optimization Code Written in Matlab.” *Structural and Multidisciplinary Optimization*, Vol. 21, No. 2, 2001, pp. 120–127. https://doi.org/10.1007/s001580050176.

[4] Liu, J., Gaynor, A. T., Chen, S., Kang, Z., Suresh, K., Takezawa, A., Li, L., Kato, J., Tang, J., Wang, C. C. L., Cheng, L., Liang, X., and To, A. C. “Current and Future Trends in Topology Optimization for Additive Manufacturing.” *Structural and Multidisciplinary Optimization*, Vol. 57, No. 6, 2018, pp. 2457–2483. https://doi.org/10.1007/s00158-018-1994-3.

[5] Zegard, T., and Paulino, G. H. “Bridging Topology Optimization and Additive Manufacturing.” *Structural and Multidisciplinary Optimization*, Vol. 53, No. 1, 2016, pp. 175–192. https://doi.org/10.1007/s00158-015-1274-4.

[6] Gaynor, A. T., and Guest, J. K. “Topology Optimization Considering Overhang Constraints: Eliminating Sacrificial Support Material in Additive Manufacturing through Design.” *Structural and Multidisciplinary Optimization*, Vol. 54, No. 5, 2016, pp. 1157–1172. https://doi.org/10.1007/s00158-016-1551-x.

[7] Langelaar, M. “Topology Optimization of 3D Self-Supporting Structures for Additive Manufacturing.” *Additive Manufacturing*, Vol. 12, 2016, pp. 60–70. https://doi.org/10.1016/J.ADDMA.2016.06.010.

[8] Kota, S., Joo, J., Li, Z., Rodgers, S. M., and Sniegowski, J. “Design of Compliant Mechanisms: Applications to MEMS.” *Analog Integrated Circuits and Signal Processing*, Vol. 29, No. 1, 2001, pp. 7–15. https://doi.org/10.1023/A:1011265810471.

[9] Jensen, B. D., and Howell, L. L. “Identification of Compliant Pseudo-Rigid-Body Four-Link Mechanism Configurations Resulting in Bistable Behavior .” *Journal of Mechanical Design*, Vol. 125, No. 4, 2004, pp. 701–708. https://doi.org/10.1115/1.1625399.

[10] Pluimers, P. J., Tolou, N., Jensen, B. D., Howell, L. L., and Herder, J. L. A Compliant On/Off Connection Mechanism for Preloading Statically Balanced Compliant Mechanisms. 373–377. https://doi.org/10.1115/DETC2012-71509.

[11] Sigmund, O. “On the Design of Compliant Mechanisms Using Topology Optimization.” *Mechanics of Structures and Machines*, Vol. 25, No. 4, 1997, pp. 493–524. https://doi.org/10.1080/08905459708945415.

[12] Pedersen, C. B. W., Buhl, T., and Sigmund, O. Topology Synthesis of Large-Displacement Compliant Mechanisms. *International Journal for Numerical Methods in Engineering*. 12. Volume 50, 2683–2705.

[13] Luo, Z., Chen, L., Yang, J., Zhang, Y., and Abdel-Malek, K. “Compliant Mechanism Design Using Multi-Objective Topology Optimization Scheme of Continuum Structures.” *Structural and Multidisciplinary Optimization*, Vol. 30, No. 2, 2005, pp. 142–154. https://doi.org/10.1007/s00158-004-0512-y.

[14] Li, Y., Saitou, K., and Kikuchi, N. “Topology Optimization of Thermally Actuated Compliant Mechanisms Considering Time-Transient Effect.” *Finite Elements in Analysis and Design*, 2004. https://doi.org/10.1016/j.finel.2003.05.002.

[15] Takezawa, A., Nishiwaki, S., Kitamura, M., and Silva, E. C. N. “Topology Optimization for Designing Strain-Gauge Load Cells.” *Structural and Multidisciplinary Optimization*, Vol. 42, No. 3, 2010, pp. 387–402. https://doi.org/10.1007/s00158-010-0491-0.

[16] Bendsøe, M. P. “Optimal Shape Design as a Material Distribution Problem.” *Structural optimization*, Vol. 1, No. 4, 1989, pp. 193–202. https://doi.org/10.1007/BF01650949.

[17] Yoon, G. H., Kim, Y. Y., Bendsøe, M. P., and Sigmund, O. “Hinge-Free Topology Optimization with Embedded Translation-Invariant Differentiable Wavelet Shrinkage.” *Structural and Multidisciplinary Optimization*, Vol. 27, No. 3, 2004, pp. 139–150. https://doi.org/10.1007/s00158-004-0378-z.

[18] Luo, J., Luo, Z., Chen, S., Tong, L., and Wang, M. Y. “A New Level Set Method for Systematic Design of Hinge-Free Compliant Mechanisms.” *Computer Methods in Applied Mechanics and Engineering*, Vol. 198, No. 2, 2008, pp. 318–331. https://doi.org/10.1016/J.CMA.2008.08.003.

[19] De Leon, D. M., Alexandersen, J., Jun, J. S., and Sigmund, O. “Stress-Constrained Topology Optimization for Compliant Mechanism Design.” *Structural and Multidisciplinary Optimization*, Vol. 52, No. 5, 2015, pp. 929–943. https://doi.org/10.1007/s00158-015-1279-z.

[20] Hansen, R. M. *Mechanical Design and Fabrication of Strain-Gage Balance*. 1956.

[21] Dubois, M. “Six-Component Strain-Gage Balances for Large Wind Tunnels.” *Experimental Mechanics*, Vol. 21, No. 11, 1981, pp. 401–407. https://doi.org/10.1007/BF02327141.

[22] Xia, Q., Shi, T., Liu, S., and Wang, M. Y. “A Level Set Solution to the Stress-Based Structural Shape and Topology Optimization.” *Computers and Structures*, 2012. https://doi.org/10.1016/j.compstruc.2011.10.009.

[23] Kang, M. K., Lee, S., and Kim, J. H. “Shape Optimization of a Mechanically Decoupled Six-Axis Force/Torque Sensor.” *Sensors and Actuators, A: Physical*, 2014. https://doi.org/10.1016/j.sna.2014.01.001.

[24] Kebede, G. A., Ahmad, A. R., Lee, S.-C., and Lin, C.-Y. “Decoupled Six-Axis Force–Moment Sensor with a Novel Strain Gauge Arrangement and Error Reduction Techniques.” *Sensors*, Vol. 19, No. 13, 2019. https://doi.org/10.3390/s19133012.

[25] Liang, Q., Long, J., Coppola, G., Zhang, D., and Sun, W. “Novel Decoupling Algorithm Based on Parallel Voltage Extreme Learning Machine (PV-ELM) for Six-Axis F/M Sensors.” *Robotics and Computer-Integrated Manufacturing*, 2019. https://doi.org/10.1016/j.rcim.2018.12.014.

[26] Tropea, C., and Yarin, A. L. *Handbook of Experimental Fluid Mechanics*. Springer Science & Business Media, 2007.

[27] Ewald, B. F. R. "Multi-Component Force Balances for Conventional and Cryogenic Wind Tunnels." *Measurement Science and Technology*, Vol. 11, No. 6, 2000, pp. R81–R94. https://doi.org/10.1088/0957-0233/11/6/201.

[28] Zhai, J., Ewald, B., and Hufnagel, K. An Investigation on the Interference of Internal Six-Component Wind Tunnel Balances with FEM. 1995.

[29] Swapna, L., Katta, B., and Suresh, B. S. "Shape Optimization of a Drag Force Element of a Force Transducer for Wind Tunnel Measurements." Vol. 5, 2015, pp. 33–38. https://doi.org/10.5923/c.jmea.201502.07.

[30] Skube, S., and Bennett, H. Wind Tunnel Balance and Method of Use, US 10,267,708 B2, 2019.

[31] Zhang, S., Li, X., Ma, H., and Wen, H. "Mechanical Analysis of Normal Force Interference on Axial Force Measurement for Internal Sting Balance." *Aerospace Science and Technology*, Vol. 58, 2016, pp. 351–357. https://doi.org/10.1016/j.ast.2016.08.028.

[32] Samardžic, M., Marinkovski, D., Anastasijević, Z., Curčić, D., and Rajić, Z. "An Elastic Element of the Forced Oscillation Apparatus for Dynamic Wind Tunnel Measurements." *Aerospace Science and Technology*, Vol. 50, 2016, pp. 272–280. https://doi.org/10.1016/j.ast.2016.01.011.

[33] Sigmund, O., and Maute, K. "Topology Optimization Approaches." *Structural and Multidisciplinary Optimization*, Vol. 48, No. 6, 2013, pp. 1031–1055. https://doi.org/10.1007/s00158-013-0978-6.

[34] Kirsch, U. topology/kirsch1990. pd. "On Singular Topologies in Optimum Structural Design." *Structural optimization*, Vol. 2, No. 3, 1990, pp. 133–142. https://doi.org/10.1007/BF01836562.

[35] Cheng, G., and Jiang, Z. "Study on Topology Optimization with Stress Constraints." *Engineering Optimization*, Vol. 20, No. 2, 1992, pp. 129–148. https://doi.org/10.1080/03052159208941276.

[36] Cheng, G. D., and Guo, X. "ε-Relaxed Approach in Structural Topology Optimization." *Structural optimization*, Vol. 13, No. 4, 1997, pp. 258–266. https://doi.org/10.1007/BF01197454.

[37] Bruggi, M., and Venini, P. "A Mixed FEM Approach to Stress-Constrained Topology Optimization." *International Journal for Numerical Methods in Engineering*, Vol. 73, No. 12, 2008, pp. 1693–1714. https://doi.org/10.1002/nme.2138.

[38] Yang, R. J., and Chen, C. J. "Stress-Based Topology Optimization." *Structural optimization*, Vol. 12, No. 2, 1996, pp. 98–105. https://doi.org/10.1007/BF01196941.

[39] Duysinx, P., and Sigmund, O. New Developments in Handling Stress Constraints in Optimal Material Distribution. In *7th AIAA/USAF/NASA/ISSMO Symposium on Multidisciplinary Analysis and Optimization*, 1998.

[40] Poon, N. M. K., and Martins, J. R. R. A. "An Adaptive Approach to Constraint Aggregation Using Adjoint Sensitivity Analysis." *Structural and Multidisciplinary Optimization*, Vol. 34, No. 1, 2007, pp. 61–73. https://doi.org/10.1007/s00158-006-0061-7.

[41] Yang, D., Liu, H., Zhang, W., and Li, S. "Stress-Constrained Topology Optimization Based on Maximum Stress Measures." *Computers and Structures*, 2018. https://doi.org/10.1016/j.compstruc.2018.01.008.

[42] Le, C., Norato, J., Bruns, T., Ha, C., and Tortorelli, D. "Stress-Based Topology Optimization for Continua." *Structural and Multidisciplinary Optimization*, Vol. 41, No. 4, 2010, pp. 605–620. https://doi.org/10.1007/s00158-009-0440-y.

[43] Kiyono, C. Y., Vatanabe, S. L., Silva, E. C. N., and Reddy, J. N. "A New Multi-p-Norm Formulation Approach for Stress-Based Topology Optimization Design." *Composite Structures*, 2016. https://doi.org/10.1016/j.compstruct.2016.05.058.

[44] Guo, X., Zhang, W. S., Wang, M. Y., and Wei, P. "Stress-Related Topology Optimization via Level Set Approach." *Computer Methods in Applied Mechanics and Engineering*, 2011. https://doi.org/10.1016/j.cma.2011.08.016.

[45] Burns, D. E., Kudzal, A., McWilliams, B., Manjarres, J., Hedges, D., and Parker, P. A. "Investigating Additively Manufactured 17-4 PH for Structural Applications." *Journal of Materials Engineering and Performance*, Vol. 28, No. 8, 2019, pp. 4943–4951. https://doi.org/10.1007/s11665-019-04206-9.

[46] Burns, D. E., and Parker, P. A. "Additively Manufactured Wind-Tunnel Balance." *Journal of Aircraft*, 2020, pp. 1–6. https://doi.org/10.2514/1.C035889.

[47] Sigmund, O., and Petersson, J. "Numerical Instabilities in Topology Optimization: A Survey on Procedures Dealing with Checkerboards, Mesh-Dependencies and Local Minima." *Structural optimization*, Vol. 16, No. 1, 1998, pp. 68–75. https://doi.org/10.1007/BF01214002.

[48] Jang, G.-W., Jeong, J. H., Kim, Y. Y., Sheen, D., Park, C., and Kim, M.-N. "Checkerboard-Free Topology Optimization Using Non-Conforming Finite Elements." *International Journal for Numerical Methods in Engineering*, Vol. 57, No. 12, 2003, pp. 1717–1735. https://doi.org/10.1002/nme.738.

[49] Bruns, T. E., and Tortorelli, D. A. "Topology Optimization of Non-Linear Elastic Structures and Compliant Mechanisms." *Computer Methods in Applied Mechanics and Engineering*, 2001. https://doi.org/10.1016/S0045-7825(00)00278-4.

[50] Guest, J. K., Prévost, J. H., and Belytschko, T. "Achieving Minimum Length Scale in Topology Optimization Using Nodal Design Variables and Projection Functions." *International Journal for Numerical Methods in Engineering*, Vol. 61, No. 2, 2004, pp. 238–254. https://doi.org/10.1002/nme.1064.

[51] Sigmund, O. "Morphology-Based Black and White Filters for Topology Optimization." *Structural and Multidisciplinary Optimization*, Vol. 33, Nos. 4–5, 2007, pp. 401–424. https://doi.org/10.1007/s00158-006-0087-x.

[52] Guest, J. K., Asadpoure, A., and Ha, S. H. "Eliminating Beta-Continuation from Heaviside Projection and Density Filter Algorithms." *Structural and Multidisciplinary Optimization*, Vol. 44, No. 4, 2011, pp. 443–453. https://doi.org/10.1007/s00158-011-0676-1.

[53] Duysinx, P., and Bendsøe, M. P. "Topology Optimization of Continuum Structures with Local Stress Constraints." *International Journal for Numerical Methods in Engineering*, Vol. 43, No. 8, 1998, pp. 1453–1478. https://doi.org/doi:10.1002/(SICI)1097-0207(19981230)43:8<1453::AID-NME480>3.0.CO;2-2.